International Journal of GEOMATE, June, 2026 Vol.30, Issue 142, pp.1-9
ISSN: 2186-2982 (P), 2186-2990 (O), Japan, DOI: https://doi.org/10.21660/2026.142.5028
Geotechnique, Construction Materials and Environment

A SEMI-ANALYTICAL METHOD FOR EMBEDDED DEPTH STABILITY OF STABILISING PILES IN FOUNDATION PIT CONSIDERING UNSATURATED EFFECTS

Long Wang[1], You Gao[2], Enquan Zhou[3], Lu Guo[1] and *Fangzhi Zhu[1]

[1]School of Civil Engineering and Architecture, Suqian University, Suqian, Jiangsu 223800, China; [2]School of Civil and Environmental Engineering, Ningbo University, Ningbo 315211, China; [3]Faculty of Civil Engineering and Mechanics, Jiangsu University, Zhenjiang 212013, China

*Corresponding Author, Received: 25 April 2025, Revised: 16 Oct. 2025, Accepted: 09 Nov. 2025

ABSTRACT: The soil bears pronounced unsaturated features as the foundation pit being larger and deeper. This study aims to investigate the influence of suction on the stability evaluation of foundation pit projects. In the category of upper bound limit analysis theorem, a straight and logarithmic spiral line combined mechanism is employed to simulate the slip surface and a horizontal slice method is advised to formulate the energy balance equation. The errors between this paper and the benchmark solution are generally less than 2.0% when the soil mass is discretized into 200 layers, indicating the satisfactory performance of the horizontal slice method and the agreement with engineering requirements. Parametric analyses are conducted and the findings indicate that the stability of foundation pit in fine-/coarse-grained soils would be underestimated/overestimated when suction is not considered in analyses. The foundation pit in fine-grained soils is more sensitive to water infiltrations. Factor of safety (FOS) drops 34.90% for SWCC-D and 16.40% for SWCC-C. For deeper foundation pits, FOS increases nearly linearly with respect to the embedded depth ratio H_2/H and the brace height ratio H_1/H. The findings provide insights into the role of suction on the foundation pit stability. This semi-analytical method can serve as an effective tool for stability analyses of unsaturated foundation pits.

Keywords: Foundation Pit, Unsaturated Soil, Limit Analysis, Embedded Depth Stability

1. INTRODUCTION

Foundation pit is an indispensable component of building and underground engineerings. As the urbanization process proceeds, the land resources become increasingly scarce and in return more and more large and deep foundation pits emerges [1]. The foundation pit design becomes more complex and significant technical challenges arise during the construction stage [2]. Hence, to ensure the safety of foundation pits and nearby buildings, more attention is required and multiple verifications, including the deformation calculation of foundation pit [3], the strength design of supporting structures and the stability assessments, should be performed during the construction stage.

For the stability issues, the embedded depth stability, the overall stability and the anti-bulge stability, should be verified and different methods, including numerical simulations, limit equilibrium and limit analysis methods [4], can all be used to address these stability problems. According to limit equilibrium principle, Xiao W., Zhou X. and Gu K. [5] recently presents a modified method to calculate the FOS of narrow foundation pits in heterogeneous soils. The calculated results show an agreement with the model tests but neglecting the influences of matric suction.

The soil in engineering practice exhibits obvious unsaturated features universally. In addition to soil particles and pore water, the presence of gas in soils makes the properties of soil more complex. The hydraulic and mechanical properties of unsaturated soils differ with those of saturated soils significantly [6]. Therefore, the unsaturated effects, characterized by soil suction, becomes more prominent and can hardly be ignored in the stability problems. For slope stability issues, recent studies indicated that, when soil suction is not considered in the analyses, the slope stability is underestimated by 4% ~ 16% [7]. Similarly, the foundation pit stability would also be underestimated when soil suction is not considered and the security reserve can hardly be determined explicitly.

Following the Mohr-Coulomb yield function and the associated flow law, the upper bound limit analysis theorem, has been proved to be an efficient tool to address the stability problems of geotechnical structures, specifically for homogeneous soils [8]. For heterogeneous materials, e.g., unsaturated soils, however, establishing the energy balance equation becomes more elaborated, resulting the difficulty in obtaining an analytical solution, especially for 3D cases [9,10]. Therefore, documents on the embedded depth stability of foundation pit in unsaturated soils using limit analysis method are insufficient. To address the unsaturated soils, spatial discretization techniques, such as the finite-element limit analysis approach [11] that combined the limit theorems with finite elements or the layer-wise summation method

[12] based on divergence theorem and superposition principle have been approved to be more effective tools. Compared with the robust finite element limit analysis method that discretizing the soil mass into numerous elements and the theoretical analysis approach that assuming a single soil block, the layer-wise summation method is moderate in terms of computational efficiency.

In this paper, a straight and logarithmic spiral line combined mechanism is used for the stability analysis of unsaturated foundation pit. To account for the suction effect, the layer-wise summation method is further modified to calculated the sliding and anti-sliding moments arising from the active and passive zones. The factor of safety in semi-analytical forms is formulated. Comparisons with benchmark results are then conducted, following by parametric analyses regarding on the roles of suction effect, phreatic line and infiltration rate on foundation pit stability. The findings in this paper can provide some guidance and reference for the design and construction of foundation pits.

2. RESEARCH SIGNIFICANCE

Foundation pit stability relates to the supported structures closely. To provide more realistic results of the foundation pit stability, the suction in soils should be considered in the analysis. However, the contribution of soil suction to foundation pit stability have not been addressed adequately in previous studies. This paper aims to study the role of suction in foundation pit stability assessments. A horizontal slice method is suggested to formulate the energy balance equation in the category of upper bound limit analysis method. Parametric analyses are conducted and the findings provide an insight into the role of suction on foundation pit stability. The proposed method can serve as an effective tool for the stability analyses of unsaturated geotechnical structures and can be further modified to address 3D cases.

3. BACKGROUND

3.1 Unsaturated Foundation Pit

The foundation pit stability relates to many factors, such as the foundation configuration (e.g., the length-width ratio and the breadth-depth ratio), the supported structures, the hydrological conditions and even the time effect [13]. For foundation pit supported by stabilizing piles, the verification of pile embedded depth is essential to guarantee the safety of foundation pit.

The earth pressure distribution behind retaining structure relates to its displacement modes and a nonlinear relationship exists [14]. Compared with a linear slip surface, a nonlinear one, especially for the logarithmic spiral surface, has been proved to be the most realistic one according to the theoretical and experimental studies [15]. For foundation pit, model tests and numerical studies indicate that the sliding surface presents a curve and straight-line combined shape [16,17].

Therefore, a straight and logarithmic spiral line combined mechanism is employed for the stability analysis of unsaturated foundation pit, as shown in Fig.1. The soil is assumed to be ideal elastic-plastic materials, govern by Mohr-Coulomb yield criterion, satisfying the normality flow rule. Limit state of the foundation pit with small deformation is studied and an energy balance equation can be established to obtain the factor of safety of the foundation pit.

The foundation pit depth is H and the supported structure embedded depth is H_2, as depicted in the graph. Only one brace is considered in the analysis and the vertical distance between the brace and the foundation pit bottom is H_1. It is assumed that the phreatic line distributes horizontally after dewatering and locates below the pile with a vertical distance z_0, dividing the soil into saturated and unsaturated zones. It should be clarified that though the whole phreatic line presents a funnel shape, a horizontal assumption can greatly simplify the analysis and facilitate the calculation and meanwhile yield satisfactory results.

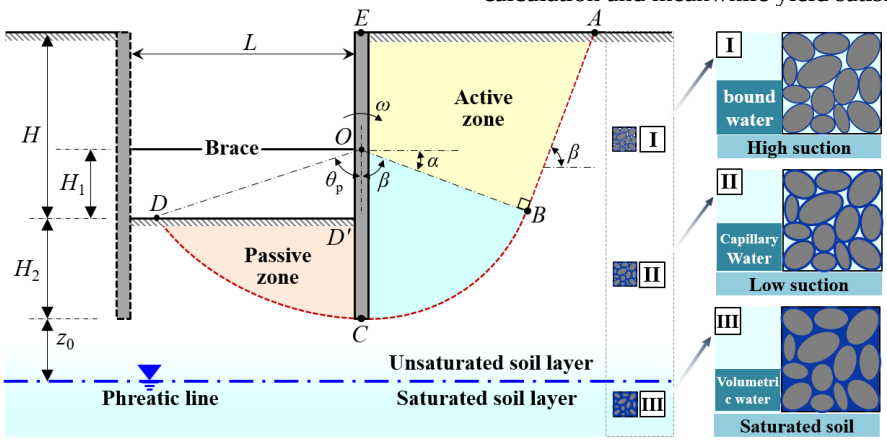

Fig.1 Mechanical model for stability analysis of foundation pit in unsaturated soils

The soil inside and outside of the foundation pit are passive and active zones, respectively. Due to the earth pressure outside the foundation pit, the supported structure tends to rotate clockwise around the support point with an angular velocity ω. In the passive zone, the slip surface remains a logarithmic spiral line that defined by a rotation angle θ_p. In the active zone, the slip surface resembles a combined straight line (with an angle of β measured from the horizontal surface, $\beta = \pi/4 + \phi'/2$, ϕ' is soil friction angle) and a logarithmic spiral line described by a rotation angle β. Because of the continuity of the soil movement, the straight and logarithmic spiral sliding surfaces in the active zone connect continuously and smoothly.

It should be noted that, in present analysis, it assumed that the foundation pit is large enough to incorporate the slip surface CD inside the foundation pit, i.e., this slip surface intersects the foundation bottom rather than the piles. When the foundation pit width is reduced, this slip surface intersects the piles and the foundation pit stability would be improved slightly. For narrower foundation pits, some adjustments are required for the proposed horizontal slice method in this paper to address this condition.

3.2 Unsaturated Soils

The behavior of unsaturated soil has been proved to follow the Mohr-Coulomb failure criteria by numerous experimental tests. The enhancement in soil strength due to soil suction is usually treated as a cohesion value. With this treatment, the studies on the stability of geotechnical structures can be greatly simplified. This cohesion value (i.e., the capillary cohesion) can be expressed as a function of the matric suction ψ using the soil water characteristic curve (SWCC) as [18]

$$c_{cap} = \psi \left[\left(\frac{\theta_w - \theta_r}{\theta_s - \theta_r} \right) \tan\phi' \right] \quad (1)$$

where θ_w, θ_s and θ_r are volumetric, saturated and residual volumetric water content, respectively. The saturated volumetric water content can be derived according to the saturated and dry unit soil weight γ_{sat} and γ_d as $\theta_s = (\gamma_{sat} - \gamma_d)/\gamma_w$.

The volumetric water content of soils can be described as [6]

$$\theta_w = \left\{ 1 - \frac{\ln(1+\psi/\psi_r)}{\ln(1+10^6/\psi_r)} \right\} \frac{\theta_s}{\left\{ \ln\left[e + (\psi/a_f)^{n_f} \right] \right\}^{m_f}} \quad (2)$$

where ψ_r is residual matric suction; m_f, n_f and a_f are fitting parameters of SWCC.

The unsteady motion in unsaturated porous media, such as soils, can be described by using a partial differential equation, i.e. the Richard Equation. For foundation pits with a depth larger than 2.0 m, the matric suction remains constant over time and varies along soil depth merely. For steady flow conditions, the matric suction can be expressed as a function of spatial variable z, i.e.,

$$\psi = -\frac{1}{\alpha} \ln\left[(1 + q/k_s)\, e^{-\alpha\gamma_w z} - q/k_s \right] \quad (3)$$

where α relates to air-entry pressure; q/k_s is specific discharge (negative and positive values represent infiltration and evaporation, respectively); γ_w is unit weight of water; z is vertical depth above the phreatic line. For the issued unsaturated foundation pit, the soil unit weight can be expressed as $\gamma' = \gamma_d + \theta_w \gamma_w$.

4. FORMULA DERIVATION

4.1 A Horizontal Slice Method

The supported structure rotates clockwise around point O under the action of internal and external earth pressures. The sliding and anti-sliding moments M_a and M_p are generated due to the active and passive zones, respectively, and can be derived from the work rate balance equations. To calculate the work rates of soil gravity and the work dissipation rates of soil cohesion, a horizontal slice method is advised, as shown in Fig.2.

It should be noted that, the adaptive meshing method can also be employed to address the issued problems. However, the proposed horizontal slice method bears a clearer physical base and a concise calculation process, facilitating the code compiling greatly and no iterations are required. Furthermore, in the derivation process, no differentiation or partial differentiation operation is involved and hence non-convergence never occurs during the calculations.

The active zone ABCE is firstly divided into soil blocks ABB'E and BCB'. The soil block ABB'E is subsequently discretized into n horizontal soil layers equally along the vertical direction and each soil layer remains a trapezoidal shape. Finally, the angles β and θ_p are discretized into n units equally, and the soil blocks BCB' and CDD' are divided horizontally according to these units.

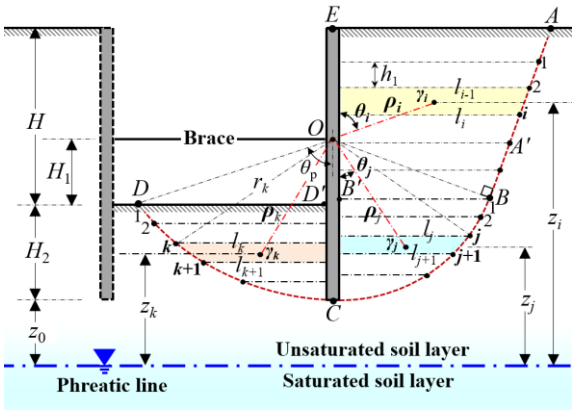

Fig.2 A horizontal slice method to calculate the work rate of soil gravity

4.2 Sliding Moment M_a

The sliding moment M_a can be derived from the energy balance equation of the active zone, i.e.,

$$W_\sigma + W_\tau = W_{\gamma'}^{\mathrm{ABB'E}} + W_{\gamma'}^{\mathrm{BCB'}} - D_c^{\mathrm{AB}} - D_c^{\mathrm{BC}} \quad (4)$$

where W_σ and W_τ are work rates done by normal and shear stresses; W_τ = 0, as the shear stress passes through the moment point O. The terms on the right side of the equation denote the work rates of soil gravity and the energy dissipation rates of soil cohesion.

For soil block ABB'E, the layer thickness is $h = \overline{\mathrm{B'E}}/n$ and the unit soil weight at the centroid of each soil layer is $\gamma_i(z_i)$. By accumulating the work rate of each soil layer, the total work rate of soil gravity can be found as:

$$W_{\gamma'}^{\mathrm{ABB'E}} = \sum_{i=1}^{n} \gamma_i(z_i) S_i \rho_i \omega \sin\theta_i \quad (5)$$

where z_i is vertical distance measured from the layer centroid to the phreatic line; S_i is area of each soil layer; ρ_i and θ_i are polar diameter and angle relates to the centroid of each soil layer, as depicted in Fig.2. Detailed expressions of these variables can be found in APPENDIX.

For soil block BCB', the rotation angle β is discretized equally into n sections (the angle element is $\Delta\theta = \beta/n$) and the soil mass is subsequently discretized into n horizontal soil layers. Similarly, the unit soil weight at the layer centroid is $\gamma_j(z_j)$. By accumulating the work rate of each soil layer, the total work rate of soil gravity can be found as:

$$W_{\gamma'}^{\mathrm{BCB'}} = \sum_{j=1}^{n} \gamma_j(z_j) S_j \rho_j \omega \sin\theta_j \quad (6)$$

where z_j is vertical distance from the layer centroid to the phreatic line; S_j is area of each soil layer; ρ_j and θ_j are polar diameter and angle relates to the centroid, as depicted in Fig.2. Detailed expressions of these variables can be found in APPENDIX.

The energy dissipated along the straight line AB and the logarithmic spiral line BC, as shown in Fig.3. The energy dissipation of an infinitesimal sliding surface can be expressed as a product of the sliding surface, its apparent cohesion and the corresponding tangential velocity components. Integrating along the entire sliding surface, the total energy dissipation rate of soil cohesion can be obtained.

For the line AB, the total energy dissipation rate becomes:

$$D_c^{\mathrm{AB}} = \int_0^{\theta_t} \left[c' + c_{\mathrm{cap}}(z_1) \right] \rho_c \cos\theta \omega ds \quad (7)$$

where $c_{\mathrm{cap}}(z_1)$ is cohesion along the sliding surface; z_1 is vertical distance to the phreatic line, as depicted in Fig.3; ds denotes the length of an infinitesimal sliding surface; ρ_c denotes the polar diameter of this infinitesimal sliding surface to point O; θ_t represents angle AOB. These variables can also be found in APPENDIX.

For the logarithmic spiral line BC, the total energy dissipation rate is:

$$D_c^{\mathrm{BC}} = \int_0^{\beta} \left[c' + c_{\mathrm{cap}}(z_2) \right] (H_1 + H_2) \mathrm{e}^{-2\theta\tan\phi'} \omega d\theta \quad (8)$$

where $c_{\mathrm{cap}}(z_2)$ is cohesion along the sliding surface; z_2 is vertical distance to the phreatic line and can be found in APPENDIX.

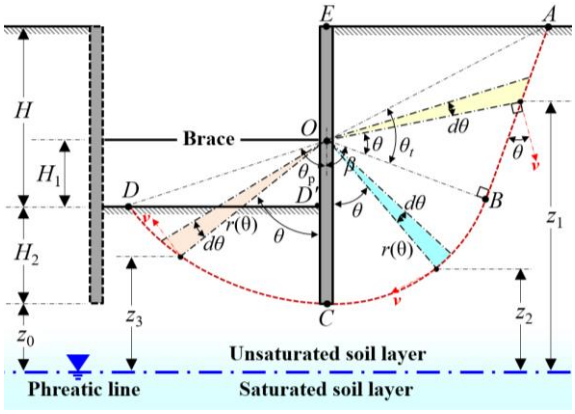

Fig.3 Calculation of the energy dissipation rate due to cohesion

4.3 Anti-Sliding Moment M_p

Similarly, the anti-sliding moment M_p can be obtained according to the energy balance equation of the passive zone, i.e.,

$$W_\sigma + W_\tau = W_{\gamma'}^{\mathrm{CDD'}} - D_c^{\mathrm{CD}} \quad (9)$$

The work rate done by shear stress is zero as the shear stress also passes through the moment point O. The terms on the right side of this equation are work rate of soil gravity and the energy dissipation rate.

According to the horizontal slice method, the rotation angle θ_p corresponding to soil block CDD' is discretized equally into n sections (the angle element is $\Delta\theta = \theta_p/n$). The total work rate of soil gravity is:

$$W_{\gamma'}^{\mathrm{CDD'}} = \sum_{k=1}^{n} \gamma_k(z_k) S_k \rho_k \omega \sin\theta_k \quad (10)$$

where $\gamma_k(z_k)$ is unit soil weight at the layer centroid; z_k is vertical distance to the phreatic line; S_k is area of each soil layer, as depicted in Fig.2; ρ_k and θ_k are polar diameter and angle from the centroid of each soil layer. These variables can also be found in APPENDIX.

The total energy dissipation rate due to cohesion along logarithmic spiral line CD is:

$$D_c^{\mathrm{CD}} = \int_0^{\theta_p} \left[c' + c_{\mathrm{cap}}(z_3) \right] (H_1 + H_2) \mathrm{e}^{2\theta\tan\phi'} \omega d\theta \quad (11)$$

where z_3 is vertical distance to the phreatic line and can be found in APPENDIX.

According to the upper bound limit analysis method and the combined line and logarithmic spiral sliding surface, the embedded depth stability can be expressed using the factor of safety (FOS) as a ratio between the anti-sliding moment and the sliding

moment, i.e., $\mathrm{FOS} = M_p / M_a$.

5. RESULTS

5.1 Comparisons

A classical foundation pit was studied to validate the proposed method. The parameters are H = 10.27 m, H_1 = 4.27 m, H_2 = 23.40 m, γ_{sat} = 17.70 kN/m^3, γ_d = 15.20 kN/m^3, c = 17.70 kPa, ϕ' = 10°, z_0 = 2.00 m. For no suction cases, the solutions obtained by this study and the benchmark solutions [5] are both list in Table 1.

It can be found evidently that FOS drops sharply at first and then declines slowly and approaches a constant value as the layer number n increases. This constant value is here selected as a benchmark value and the other FOS is normalized this benchmark value, as list in the table. For n > 200, FOS becomes insensitive to the layer number and the error is less than 2.00%. The solutions in this paper agrees with the published one, illustrating the feasibility and applicability of the proposed method in the safety assessments.

It should be clarified that the convergence of the proposed method depends closely on soil strength parameters and the slope configurations [10]. The method converges satisfactorily for 200 layers and the errors can meet the engineering requirements. Therefore, in the following analyses, a layer number of n = 200 is used in the embedded depth stability analysis of unsaturated foundation pit.

Table 1 Relations between FOS and layer number n

	Layer number n				Published results [5]
	100	200	300	400	
FOS	1.403	1.394	1.391	1.390	1.371
Error (%)	2.334	1.678	1.459	1.386	0.000

5.2 Suction Effect

The previous foundation pit is investigated and the suction is considered in the following analyses. Four selected SWCC curves, covering a wider range of unsaturated soils in engineering practice, are used and the corresponding parameters are listed in Table 2 [19]. Generally, SWCC A and B represent coarse-grain soils, C and D represent fine-grain soils.

The safety factor increases nearly linearly as H_1 increases and nonlinearly as H_2 increases as shown in Fig.4. This means that the foundation pit becomes more stable when the brace is placed on the upper portion of the foundation pit. The deeper the brace is embedded, the more stable the foundation pit tends to be. It is interesting to be noted form the graph that FOS depends on soil types closely. The stability of foundation pit in fine-grained soils is enhanced, but is reduced in coarse-grained soils. This implies that the stability of foundation pit in fine-/coarse-grained soils would be underestimated/overestimated when suction is not considered in the analysis. The suction effect in fine-grained soils is more pronounced than that in coarse-grained soils.

Table 2 Parameters for selected SWCC curves [19]

SWCC No.	a_f (kPa)	n_f	m_f	ψ_r (kPa)	α_f (kPa^{-1})	θ_r
A	1	2	1	10	2.000	0.081
B	10	2	1	100	0.200	0.080
C	100	2	1	1000	0.020	0.078
D	1000	2	1	10000	0.002	0.073

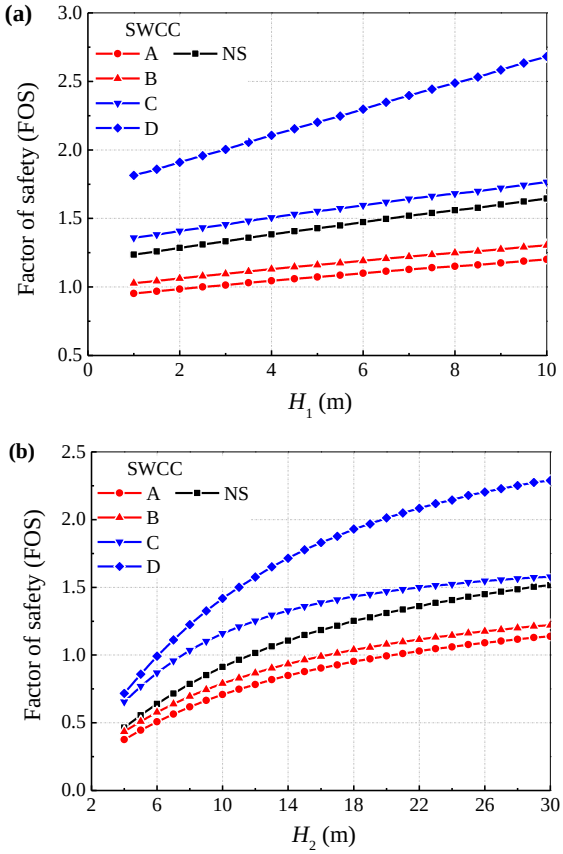

Fig.4 Relations between safety factor FOS and parameter (a) H_1 and (b) H_2

5.3 Influences of c and ϕ'

The safety factor increases nearly linearly with the increase of c and nonlinearly with the increase of ϕ', as shown in Fig.5. Similarly, the suction effect plays a positive role in fine-grained soils, but a negative role in coarse-grained soils. The suction effect is more insensitive to soil friction angle, but is relatively insensitive to soil cohesion. This is due to the fact that the capillary cohesion, as expressed in equation 1, relates closely to the soil friction angle

and SWCC, but is independent on soil cohesion. When the friction angle is fixed (Figure 5a), the cohesion effect appears independent of soil cohesion. Conversely, when the cohesion is fixed (Figure 5b), the cohesion effect differs remarkably as the friction angle increases. The suction effect nearly vanishes as ϕ' approaches zero.

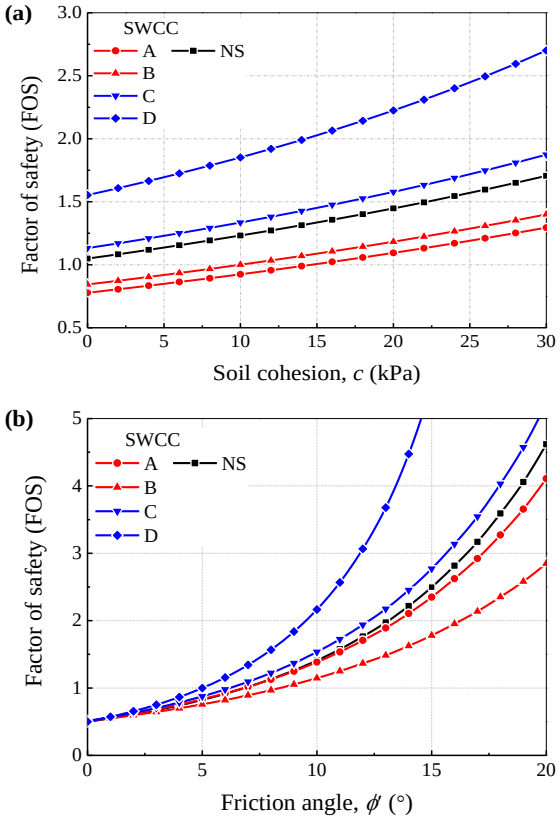

Fig.5 Relations between safety factor FOS and parameter (a) c' and (b) ϕ'

5.4 Influence of Infiltration Rate

Fig.6(a) shows the infiltration rate q/k_s on the foundation pit stability. As expected, the foundation pit stability declines as the infiltration rate increases and finally approaches the no suction cases as q/k_s = -1. Fine-grained soil is more sensitive to infiltration rate; FOS drops 34.90% for SWCC-D and 16.40% for SWCC-C. Therefore, specific attention should be paid to the infiltration rate, as it is one of the most important factors affecting the foundation pit stability, especially in fine-grained soils. The finer the soil is, the more significant the impact of infiltration on the foundation pit stability becomes. Conversely, for coarse-grained soils, FOS drops only 3.58% for SWCC-B and 0.47% for SWCC-A. This means that if the foundation pit locates in coarse-grained soils, the influence of infiltration rate on its stability can nearly be ignored. The coarser the soil is, the smaller the impact of infiltration on the foundation pit stability becomes.

5.5 Influence of Phreatic Line

The phreatic line depth possesses significant impact on the foundation pit stability and also relates closely to soil types, as depicted in Fig.6(b). The stability of foundation pit in coarse-grained soils declines gradually as the phreatic line drops. FOS drops 14.70% for SWCC-A and 9.55% for SWCC-B. This is consistent with the findings reported by model tests and numerical simulations that the slope stability decreases as the reservoir water level drops [20, 21]. Conversely, for SWCC-D, the foundation pit stability is enhanced linearly as the phreatic line drops. FOS is increased by 21.50% as the phreatic line drops from z_0 = 2 m to z_0 = 10 m. For SWCC-C, though presents fine-grained soils, the foundation pit stability also declines as the phreatic line drops (FOS drops 4.56%). This is because that the unit soil weight and cohesion profile along soil depth varies dramatically as the phreatic line drops, resulting the alteration of the foundation pit stability. The pore water pressure dissipates and the effective stress increases as the water level drops, causing soil shear shrinkage deformation. Furthermore, the reduction in matric suction reduces the soil shear strength and the penetration due to the seepage also affect the slope stability.

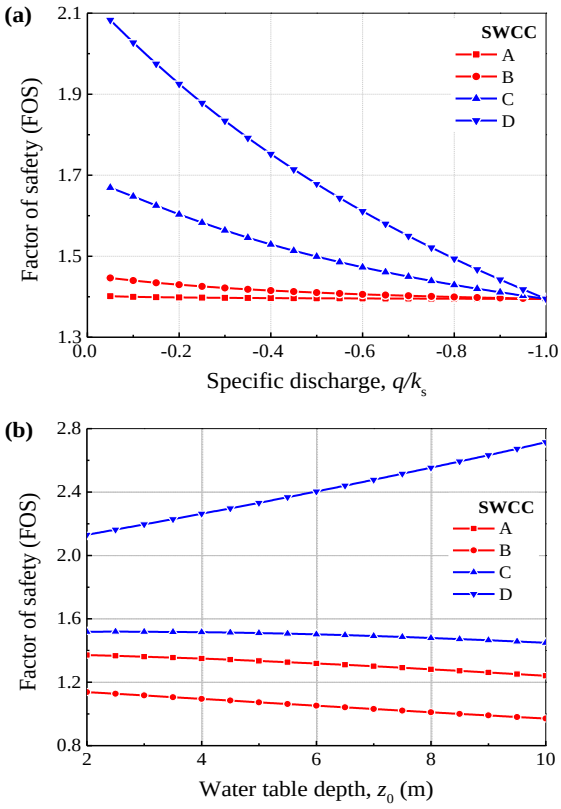

Fig.6 Relations between safety factor FOS and (a) infiltration rate and (b) phreatic line depth

5.6 Influence of H_2/H and H_1/H

Fig.7 presents the relations between FOS and the embedded depth ratio H_2/H and the brace height ratio H_1/H, respectively. The SWCC-C is adopted and the foundation pit depth varies from H = 4 m to 12 m. The results without considering soil suction are also plotted in the graph for comparisons. For deeper foundation pits, FOS increases as the embedded depth ratio increase universally whether the soil suction is considered or not in the analysis. However, the growth rate of FOS with respect to H_2/H presents different patterns as the foundation pit depth increases. A linear growth pattern for deep foundation pit and a nonlinear growth pattern for shallow foundation pit can be observed evidently. For extremely shallow foundation pit, such as H = 4 m, FOS increases sharply at first and then decreases slowly as the embedded depth increases.

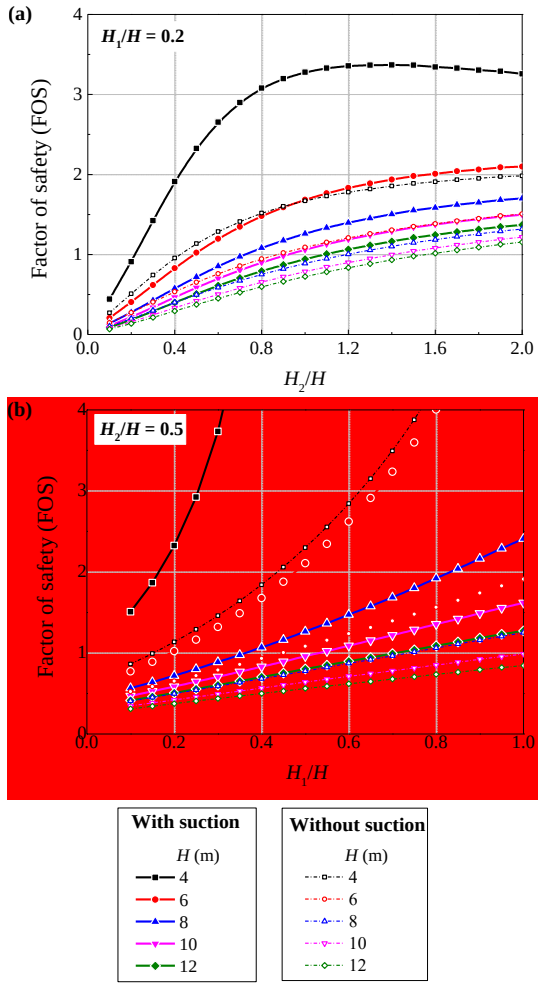

Fig.7 Relations between safety factor FOS and (a) H_2/H (H_1/H = 0.2) and (b) H_1/H (H_2/H = 0.5)

This is because that the phreatic line is assumed to be located beneath the supporting structure. The phreatic line drops as the embedded depth increase and a decrease in FOS can be observed for SWCC-C as shown in Fig.6(b). The foundation pit stability is improved evidently as the brace moves from the pit bottom to the ground surface, as shown in Fig.7(b). This is because that the force arm for passive zones increases more evidently compared with that of active zones. For deeper foundation pits, FOS increases linearly with respect to the brace height. For shallower foundation pits, however, FOS is more sensitive to the brace height.

6. CONCLUSION

A straight and logarithmic spiral line combined mechanism is used to simulate the potential slip surface and a horizontal slice method is advised to formulate the energy balance equation in the category of upper bound limit analysis theorem. The external work rate of soil gravity is calculated and the factor of safety are obtained and compared with the published solutions, indicating the validity of this method. The method converges rapidly as the layer number increases and the error is generally less than 2.00% for a layer number of n > 200.

1) The foundation pit stability relates closely to soil types. The stability of foundation pit in fine-/coarse-grained soils is nderestimated/overestimated when the suction is not considered. The suction effect in fine-grained soils is more pronounced than that in coarse-grained soils.

2) The suction effect is more insensitive to soil friction angle, but is relatively insensitive to soil cohesion. The suction effect nearly vanishes as ϕ' approaches zero. Fine-grained soil is more sensitive to the infiltration rate, and the influence of infiltration rate on the stability issues cannot be ignored. For coarse-grained soils, the influence of infiltration rate on the stability of foundation pit can nearly be ignored.

3) As the phreatic line drops, the stability of foundation pit is generally reduced for coarse-grained soils. For fine-grained soils, the influence of phreatic line variation on foundation pit stability depends on specific SWCC. For deeper foundation pits, FOS increases nearly linearly with respect to the embedded depth ratio H_2/H and the brace height ratio H_1/H. For shallower foundation pits, FOS is more sensitive to H_2/H and H_1/H.

The proposed method can serve as an effective tool to evaluate the embedded depth of stabilizing piles in unsaturated foundation pit. Additionally, the approach can be further modified to assess the basal heave stability of foundation pit and even for 3D unsaturated foundation pits.

7. ACKNOWLEDGMENTS

This research was performed with the financial support from National Natural Science Foundation of China (Grant No. 52208345, 52268054).

8. APPENDIX

The variables z_i, ρ_i, θ_i and S_i in equation 5 can be expressed as:

$$z_i = z_0 + H_2 + H - (i-0.5)h \qquad i = 1...n \tag{1}$$

$$\rho_i = \sqrt{(0.5l_{i-0.5})^2 + \left[(H-H_1)-(i-0.5)h\right]^2} \tag{2}$$

$$\theta_i = \arctan\frac{0.5l_{i-0.5}}{(H-H_1)-(i-0.5)h} \tag{3}$$

$$S_i = 0.5h(l_{i-1} + l_i) \tag{4}$$

where l_i and l_{i-1} are the upper and lower surface of each layer. The width of the foundation is taken as unit and l_i can be expressed as:

$$l_i = (H_1 + H_2)\mathrm{e}^{-\beta\tan\phi'}\cos\alpha + \left\{H - H_1 + (H_1 + H_2)\mathrm{e}^{-\beta\tan\phi'}\sin\alpha\right\}\tan\alpha - (i-1)h\tan\alpha \tag{5}$$

The variables z_j, ρ_j, θ_j and S_j in equation 6 can be expressed as:

$$z_j = z_0 + H_2 + H_1 - r_{j+0.5}\cos\left[(j+0.5)\Delta\theta\right] \qquad j = 1...n \tag{6}$$

$$\rho_j = \sqrt{\left\{0.25(l_j + l_{j+1})\right\}^2 + \left\{r_{j+0.5}\cos(j+0.5)\Delta\theta\right\}^2} \tag{7}$$

$$\theta_j = \arctan\frac{0.25(l_j + l_{j+1})}{r_{j+0.5}\cos(j+0.5)\Delta\theta} \tag{8}$$

$$S_j = 0.5(l_j + l_{j+1})\left\{r_j\cos j\Delta\theta - r_{j+1}\cos(j+1)\Delta\theta\right\} \tag{9}$$

where l_j and l_{j+1} are the upper and lower surface of each layer and l_j can be expressed as:

$$l_j = r_j\sin j\Delta\theta \tag{10}$$

$$r_j = (H_1 + H_2)\mathrm{e}^{-j\Delta\theta\tan\phi'} \qquad j = 1...n \tag{11}$$

The variables z_1, ds, ρ_c and θ_t in equation 7 can be expressed as:

$$z_1 = z_0 + H_2 + H_1 - (H_1 + H_2)\mathrm{e}^{-\beta\tan\phi'}(\sin\alpha - \tan\theta\cos\alpha) \tag{12}$$

$$ds = \frac{(H_1 + H_2)\mathrm{e}^{-\beta\tan\phi'}}{\cos^2\theta}d\theta \tag{13}$$

$$\rho_c = \frac{(H_1 + H_2)\mathrm{e}^{-\beta\tan\phi'}}{\cos\theta} \tag{14}$$

$$\theta_t = \arctan\frac{H - H_1 + (H_1 + H_2)\mathrm{e}^{-\beta\tan\phi'}\sin\alpha}{\cos\alpha(H_1 + H_2)\mathrm{e}^{-\beta\tan\phi'}} \tag{15}$$

The variables z_2 in equation 8 can be expressed as:

$$z_2 = z_0 + H_1 + H_2 - r(\theta)\cos\theta \tag{16}$$

The variables z_k, S_k, ρ_k and θ_k in equation 10 can be expressed as:

$$z_k = z_0 + H_2 + H_1 - \left\{r_{k+0.5}\cos(k+0.5)\Delta\theta\right\} \tag{17}$$

$$S_k = 0.5(l_k + l_{k+1})\left\{r_k\cos k\Delta\theta - r_{k+1}\cos(k+1)\Delta\theta\right\} \tag{18}$$

$$l_k = r_k\sin k\Delta\theta \tag{19}$$

$$r_k = (H_1 + H_2)\mathrm{e}^{k\Delta\theta\tan\phi'} \qquad k = 1...n \tag{20}$$

$$\rho_k = \sqrt{\left\{0.25\left(l_k + l_{k+1}\right)\right\}^2 + \left\{r_{k+0.5}\cos(k+0.5)\Delta\theta\right\}^2} \tag{21}$$

$$\theta_k = \arctan\frac{0.25\left(l_k + l_{k+1}\right)}{r_{k+0.5}\cos(k+0.5)\Delta\theta} \tag{22}$$

The variables z_3 in equation 11 can be expressed as:

$$z_3 = z_0 + H_1 + H_2 - (H_1 + H_2)\mathrm{e}^{\theta\tan\phi'}\cos\theta \tag{23}$$

9. REFERENCES

1. Dang T.X., Nguyen T.A., Tran H.V.V., Nguyen P. T. and Vo L.N., Impact of Barrette Wall Thickness on Displacement and Force in Deep Excavation Project. International Journal of GEOMATE, Vol. 28, Issue 125, 2025, pp.75-82. https://doi.org/10.21660/2025.125.4704.
2. Pham D.T., Tran N.H., Cao V.H. and Zhairbaeva G., Horizontal Strain-Slope Stability Correlation Considering the Effect of Shallow Excavation Near the Slope Toe. International Journal of GEOMATE, Vol. 27, Issue 119, 2024, pp.42-49. https://doi.org/10.21660/2024.119.4348.
3. Vuong P.Q., Tran H.T., and Nguyen T.A., Reducing the Horizontal Displacement of the Diaphragm Wall by the Active Support System in Hanoi. International Journal of GEOMATE, Vol. 25, Issue 108, 2023, pp.199-207. https://doi.org/10.21660/2023.108.3856.
4. Zhang D., Influences of Deep Foundation Pit Excavation on the Stability of Adjacent Ancient Buildings. Buildings, Vol. 13, Issue 8, 2023, pp.2004. https://doi.org/10.3390/buildings13082004.
5. Xiao W., Zhou X., Gu K., Influence of Excavation Width on “Skirt” Stability of Foundation Pits. Building Structure, Vol. 51, Issue S2, 2021, pp.1618-1623. (in Chinese)
6. Fredlund D.G. and Xing A.Q., Equations for the Soil-water Characteristic Curve. Canadian Geotechnical Journal, Vol. 31, Issue 4, 1994, pp.521-532. https://doi.org/10.1139/t94-061.
7. Zhang L.L., Fredlund M.D., Fredlund D.G., Lu H, Wilson G.W., The Influence of the Unsaturated Soil Zone on 2-D and 3-D Slope Stability Analyses. Engineering Geology, Vol. 193, 2014, pp.374-383. https://doi.org/10.1016/j.enggeo.2015.05.011.
8. Chen W.F., Limit analysis and soil plasticity. 1975, Amsterdam: Elsevier.
9. Wang L., Gao Y., Zhou E.Q., Feng J.X., Huang A.P., and Xu M.J., Pseudo-static Analysis of 3D Unsaturated Bench Slopes Reinforced with Multiple Rows of Piles. Transportation Geotechnics, Vol. 46, 2024, pp. 101255. https://doi.org/10.1016/j.trgeo.2024.101255.
10. Wang L., Hu W., Gao Y., Zhou E.Q., Li J., and Chen G.X., Estimation of 3D Earth Pressure with Inclined Backfill Surface Considering Seismic Loads and Suction Effects. International Journal

for Numerical and Analytical Methods in Geomechanics, Vol. 47, Issue 6, 2023, pp.1086-1099.
https://doi.org/10.1002/nag.3499.

11. Sloan S.W., Geotechnical Stability Analysis. Géotechnique, Vol. 63, Issue 7, 2013, pp. 531-572.
https://doi.org/10.1680/geot.12.RL.001.
12. Wang L., Chen G.X., Hu W., Zhou E.Q., Feng J.X., and Huang A.P., Seismic Stability of Expansive Soil Slopes Stabilized by Anchor Cables using A Modified Horizontal Slices Method. Earthquake Engineering and Engineering Vibration, Vol. 23, 2024, pp.377-387.
https://doi.org/10.1007/s11803-024-2242-z.
13. Wang W., Han Z., Deng J., Zhang X., and Zhang Y., Study on Soil Reinforcement Param in Deep Foundation Pit of Marshland Metro Station. Heliyon, Vol. 5, Issue 11, 2019, pp.e02836.
https://doi.org/10.1016/j.heliyon.2019.e02836.
14. Liu T., Hou T.S., and Liu H.Y., Active Earth Pressure Characteristics of Light Weight Soil with Eps Particles behind Rigid Retaining Wall. International Journal of Geosynthetics and Ground Engineering, Vol. 10, Issue 2, 2024, pp.21.
https://doi.org/10.1007/s40891-024-00527-5.
15. Liu S., Gao Z., and Li M., A Closed-form Logarithmic Spiral Method for Seismic Passive Earth Pressure in Anisotropic Sand. Computers and Geotechnics, Vol. 152, 2022, pp.105052.
https://doi.org/10.1016/j.compgeo.2022.105052.
16. Xu S.Y., Ismaillawal A.I., Shamsabadi A., and Taciroglu E., Estimation of Static Earth Pressures for A Sloping Cohesive Backfill Using Extended Rankine Theory with A Composite Log-spiral Failure Surface. Acta Geotechnica, Vol. 14, Issue 2, 2019, pp.579-594.
https://doi.org/10.1007/s11440-018-0673-2.
17. Xu S.Y., Kannangara K.K.P.M., and Taciroglu E., Analysis of the Stress Distribution Across A Retaining Wall Backfill. Computers and Geotechnics, Vol. 103, 2018, pp. 13-25.
https://doi.org/10.1016/j.compgeo.2018.07.001.
18. Vanapalli S.K., Fredlund D.G., Pufahl D.E., and Clifton A.W., Model for the Prediction of Shear Strength with Respect to Soil Suction. Canadian Geotechnical Journal, Vol. 33, Issue 3, 1996, pp.379-392.
https://doi.org/10.1139/t96-060.
19. Zhang L.L., Fredlund D.G., Fredlund M.D., and Wilson G.W., Modeling the Unsaturated Soil Zone in Slope Stability Analysis. Canadian Geotechnical Journal, Vol. 51, Issue 12, 2014, pp.1384-1398.
https://doi.org/10.1139/cgj-2013-0394.
20. Xiong X., Shi Z.M., Xiong Y.L., Peng M., Ma X.L., and Zhang Feng., Unsaturated Slope Stability around the Three Gorges Reservoir under Various Combinations of Rainfall and Water Level Fluctuation. Engineering Geology, Issue 261, 2019, pp.105231.
https://doi.org/10.1016/j.enggeo.2019.105231.
21. Meng Q.X., Qian K., Zhong L., Gu J.J., Li Y., Fan K.F., and Yan L., Numerical Analysis of Slope Stability under Reservoir Water Level Fluctuations Using A FEM-LEM-combined method. Geofluids, Vol. 2020, 2020, pp.6683311.
https://doi.org/10.1155/2020/6683311.